INSHORE-NEARSHORE MORPHODYNAMICS - A PREDICTIVE MODEL

John Chappell

Dept. of Biogeography and Geomorphology, R.S.Pac.S.,
Australian National University, Canberra, Australia.

ABSTRACT The two-dimensional topography, developed on a sandy sea bed between surf hase and the breaker zone, is computed using (i) sediment gain or loss per unit bed area = zero, (ii) simple models of sediment drift in terms of, firstly, simplified saltation under Stokesian waves, and secondly, frictional wave work on the sea bed, (iii) the drift tendency in direction of wave propogation being offset of the local sea bed gradient. An input contour line at surf base is assumed, across which the input wave train is propogated. Using standard wave refraction combined with (i) to (iii), above, an equilibrium topography is generated by iteration. Inshore of the breaker line, longshore currents generated by radiation stress are combined with the gradient effect to balance sediment drift, producing bar - trough topography.

INTRODUCTION

Nearshore bathymetric profiles commonly are modelled by concave power functions of distance from shore (eg., Le Blond, 1979), on empirical grounds (Bruun, 1962). This paper seeks to model 2-dimensional bathymetric topography in terms of shoreward sediment drift induced, in an idealised way, by shoaling waves, in opposition to the effect of a downslope (gradient) factor. In the inshore zone, the effects of longshore currents and of shore-normal rip currents on sediment movement are included, again in a simplified way. The nearshore zone is defined here as extending from the primary breaker line seawards to surf base, which is taken as the maximum depth at which sediment is likely to be moved by wave motion. The inshore zone is taken to be between the primary breaker line and the swash zone, on the beach face.

Sediment movement under shoaling waves is complex, involving both saltating grains and supension clouds, which move differently at different phases of a wave cycle and at different points above a bed ripple (eg., Neilson, 1978). Furthermore, the type of small scale bed form (ripple, megaripple, etc.) varies with depth (Boyd, this volume). The net drift tendency also varies with wave shape - a function not only of shoaling but also of wind direction relative to wave direction. As a general model of sediment drift under shoaling waves does not yet appear to exist, we commence with a highly idealised picture.

SEDIMENT DRIFT

Sediment movement is initiated when the horizontal component (u_*) of wave orbital velocity at a certain distance from the bed exceeds a critical value, u_t. This threshold value has been shown to be a discontinuous function of sediment particle size (Komar and Miller, 1975). Once movement is initiated, sediment drift generally is argued to be related to the cube of u_* (eg., Bagnold, 1966) on the grounds that mass transport should be proportional to frictional wave work (W) on the bed, where

$$W = \rho u_*^3 \quad \ldots\ldots \quad (1)$$

(Inman et al., 1966; Kachel and Sternberg, 1971). However, while the magnitude of mass transport may depend on W, the sense of direction is not indicated when u_* is estimated from the maximum of the horizontal orbital velocity component, as is conventional. An approach here is to estimate u_* by integrating instantaneous velocity through a wave cycle, although suggestions along these lines (Wells, 1967; Wright et al., 1980) so far are heuristic rather than analytic or well verified.

Shoaling waves are asymmetrical, and non-zero values of net water transport and of bed shear stress appear when Stokesian and higher order wave equations are integrated through a wave cycle. Although the magnitudes of these resultants are small compared with instantaneous values, they are likely to induce sediment drift at depths shallower than surf base, where instantaneous velocities exceed u_t for a substantial part of the wave cycle. Thus, for Stokes waves. Longuet-Higgins (1953) gives the net shoreward velocity near the bottom as

$$U_o = \frac{5}{4}\left(\frac{\pi H}{L}\right)^2 C \frac{1}{(\sinh(kh))^2} \quad \ldots\ldots\ldots \quad (2)$$

where H is local wave height, L is wavelength, C is celerity, $k=2\pi/L$, and h is depth to bed. Bed drift data of Russell and Osorio (1958) correlate quite well with U_o, although as Komar (1976) points out, it is not known whether the relationship is causal. However, setting aside the problematic interaction between small scale bed forms and sediment movement, it seems reasonable that net sediment flux is proportional to the product of the entraining factor (bed shear stress) and net velocity U_o, ie.,

$$Q_s = U_o \zeta \tau \quad \ldots\ldots\ldots \quad (3)$$

where ζ is a coupling factor and τ is effective bed shear stress. Whether $\tau \propto u_*^2$, or $\tau \propto (u_* - u_t)^2$ (cf. Wright et al., 1980) is not known; here it is taken as popoртional to u_*^2. It is noted that U_o is better calculated by using a wave equation more accurate than the Stokes model (eg., that of Fenton and Rienecker, this conference). However, eq.(2) is used in the present paper.

Net sediment drift should be influenced by bed slope. Experimental data seem not to indicate how this factor might be combined with any formulation for flux such as eq.'s (1) - (3), although Taylor and Dyer

(1977) suggest that for bedload flux

$$\vec{Q}_s(\text{bedload}) = \frac{\zeta \vec{W}}{(\tan\phi \pm \tan\beta).\cos\beta} \qquad \ldots\ldots\ldots \quad (4)$$

where ϕ is an angle of intergranular friction and β is slope angle, positive upslope. ζ has the same meaning but different value as in eq.(3). Wave hemicycle vectors ($\overleftarrow{Q}_s$, $\overrightarrow{Q}_s$, etc.) are assessed by integrating through each hemicycle.

The approach in this paper is to assume that grains have average trajectories of pathlengths $\overleftarrow{\lambda}$, $\overrightarrow{\lambda}$ in each hemicycle, and that saltating grains, on descent, make an angle α with the horizontal. It is assumed that supended grains have a net displacement of U_o per wave cycle. From figure 1, net saltation displacement comes to

$$\Lambda \simeq 2\bar{\lambda}\,\frac{\tan\beta}{\tan\alpha} \qquad \ldots\ldots\ldots \quad (5)$$

where $\bar{\lambda}$ is the mean of $\overleftarrow{\lambda}$, $\overrightarrow{\lambda}$ (without sense of sign). Hence, Λ is downslope, as β is negative in this direction. In the following section, eq's (3) and (5) are used to balance sediment drift, at the equilibrium condition.

An alternative approach is to consider sediment drift as directly proportional to wave frictional work on the bed. Friction per wave cycle per unit area is

$$F = \frac{2}{3\pi}\,\rho f\, u_{max}^3 \qquad \ldots\ldots\ldots \quad (6)$$

(Jonnson, 1965) where u_{max} is maximum instantaneous bottom orbital velocity. Although the friction coefficient, f, usually is taken as constant for a given bed sediment, Jonnson (1965) shows that it changes with horizontal length scale of bottom orbital motion, ie., is proportional to u_{max} (in turbulent motion). The frictional loss (K_f) as a function of wave height, based on a similar $F \propto u^3$ relationship, is given by Bretschneider and Reid (1954) as

$$K_f = \left(1 + \int_o^x ¶\, dx\right)^{-1} \qquad \ldots\ldots\ldots \quad (7)$$

where

$$¶ = H\,\frac{8f\,K_s}{3g^2T}\left\{\frac{\omega}{\sinh(kh)}\right\}^3 \qquad \ldots\ldots\ldots \quad (8)$$

where T is wave period and ω is $2\pi/T$. Again in the next section this is balanced against a slope-dependant drift, although in this case figure 1 and eq.(5) have no direct relevance, and the downslope component is simply

$$\Lambda' = 2\bar{\lambda}\tan\beta \qquad \ldots\ldots\ldots \quad (9)$$

EQUILIBRIUM PROFILE

Bed equilibrium occurs when sediment gain or loss per unit area is zero. This occurs when <u>either</u> there is no sediment movement to or

Figure 1: SIMPLIFIED SALTATION DRIFT. Wave hemicycles separated for clarity.

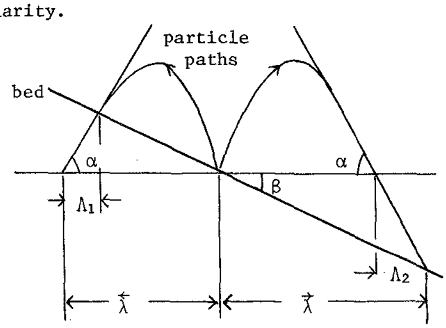

Net displacement $\Lambda = \Lambda_1 + \Lambda_2 \simeq 2\bar{\lambda}\,\dfrac{\tan\beta}{\tan\alpha}$. $(\bar{\lambda} = 0.5(|\overleftarrow{\lambda}| + |\overrightarrow{\lambda}|))$.

Figure 2: MODEL EQUILIBRIUM BED PROFILES.

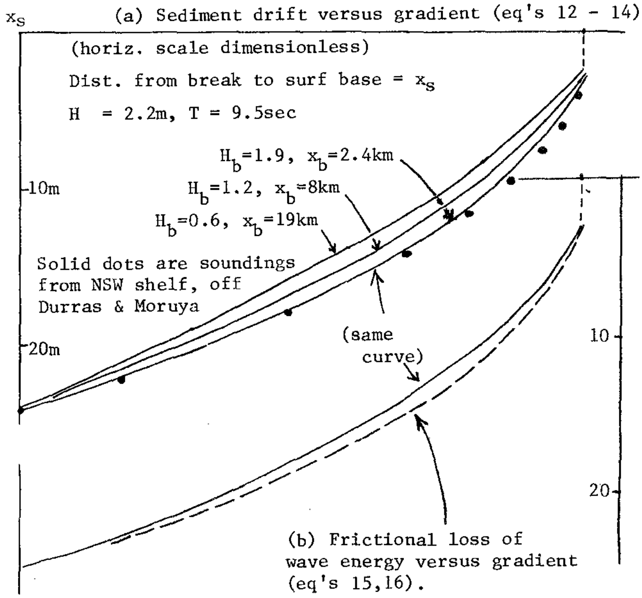

from a unit area (closed system case), or there is a constant flux along the profile (external sources and sinks case). Either way,

$$\text{grad } Q_s = \text{zero.} \qquad \ldots\ldots\ (10)$$

In what follows, the nearshore zone is considered as a closed system case, while the inshore zone can locally be regarded as a steady state case where $Q_s \neq 0$ but eq.(10) applies.

We take the nearshore zone first. From the foregoing, at equilibrium the drift Q_s according to eq.(3) is set equal and opposite to the down-slope tendency Λ in eq.(5). In the results which follow, $\bar{\lambda}$ is taken as equal to mean bed velocity

$$u_b = \frac{\pi H}{T} \frac{1}{\sinh(kh)} \qquad \ldots\ldots\ (11)$$

It is noted that a better estimate would be acheived by integrating higher order wave equations through a cycle. Similarly, τ, τ, are taken as equal and opposite, although a better estimate could also be based on higher order wave equations. In this simple formulation, zero net displacement occurs when

$$U_o = 2\bar{\lambda}\,\frac{\tan\beta}{\tan\alpha} \qquad \ldots\ldots\ (12)$$

Hence, using eq's (2), (11), (12), the bed gradient is a function of local wave height, water depth, and the unknown parameter, α. The latter may depend directly on u_{max} (in a similar way to friction coefficient, f) but initially it is assumed that α is constant, and the assumption is discussed later.

As we are seeking two dimensional topography for an arbitrary surf-base contour, wave refraction must be taken into account, and local wave height H varies from deepwater wave height H_∞ according to

$$H = H_\infty K_r K_s K_f \qquad \ldots\ldots\ (13)$$

where K_f is given at eq.(7), K_s (shoaling coefficient, also in eq.(7)) and K_r (refraction coefficient) are as given in standard works (eg., Komar, 1976).

The local profile along a given wave ray, from eq's (11) and (12) can therefore be computed from

$$\frac{dz}{dx} = \frac{5\ H\pi\tan\alpha}{8C\ \sinh(kh)} \qquad \ldots\ldots\ (14)$$

To calculate a profile, values must be assumed for f (entering eq.(13) from eq.(8), and for α. The approach used here is to assume that the overall distance from surf base to the breaker line is set by the initial width of the inner shelf (geologically determined), and the profile z(x) then calculated from (14) using f = 0.02 and α adjusted to suit. Although arbitrary in this last particular, computed profiles closely accord with actual profiles, as shown in figure 2a.

The trajectory parameter clearly subsumes other factors and, as mentioned, is likely to vary with u_b amongst other things. Although intrinsically unsatisfactory, this parametric approach is useful in tbat α can be related to objective factors, through comparisons such as in figure 2, as has been the case in the past with coefficient f.

An alternative to using the simple sediment movement model of figure 1 is to equate sediment drift with net bed friction. For example, Q_s may be directly related to W in eq.(1) (cf. Bagnold, 1966) by $Q_s = \zeta W$, and this can be opposed to a gradient force to give

$$\frac{dz}{dx} = \frac{\rho u_*^3}{\Lambda g} . \zeta$$

Using a similar idea, Chappell and Eliot (1979) used the Bretschneider and Reid frictional factor ¶ (eq.8) to offset the gradient force, arguing that frictional loss of wave energy is proportional to the sediment drift tendency, as follows. Wave height change δH over length δx is

$$\delta H = 1 - \left(\frac{fH\P\delta x}{T^4 K_s} + 1\right)^{-1} \qquad \ldots\ldots\ (15)$$

Wave energy loss, δE, is

$$\delta E = 2H\,\delta H.\ \rho g/8 \qquad \ldots\ldots\ (16)$$

and setting $dz/dx \propto \delta E$ again gives a computational solution for $z(x)$, using, as before, the wave height equation (13) as appropriate*. Figure 2b compares the result of this model with that of the more explicit sediment drift model in figure 1 and figure 2a. A disadvantage of this model, compared with the previous one, is that it does not explicitly assess frictional drift tendencies for each wave hemicycle because, as it stands, it rests on Airy waves.

Both models illustrated in figure 2 fit quite closely to the curve $z = a\,x^b$, $b<1$ (where $z=0$ is the breaker line, and z is +ve with depth), which is quite widely used to fit empirically to real nearshore profiles. However, empirical $z = a\,x^b$ has no explanatory power, whereas the arguements outlined here explicitly develop bed profile in terms of bed equilibrium assessed by sediment drift models, albeit crude ones. As the first model is the more complete, in the sense that it is based on a conception of sediment movement and that Stokes (or higher order wave equations) can be used, it is employed in the following section, where 2-dimensional topography is developed.

The inshore zone can be more complex, in that the sediment flux locally can be different from zero in the presence of rip current cells, although eq.(10) still holds. Treatment of this area is deferred to a later section.

---

* Chappell and Eliot (1979), using this type of approach, simplified the problem by assuming that frictional work on the bed is uniformly distributed at equilibrium. Empirical calculations of ¶ (eq.8) for real profiles and waves show that this is not true, and the opportunity is taken here to correct this. Following from this, it would be interesting to discover whether "entropy production" (eg., $\delta E/h_*$, $h_* = h_s - h$ where h_s is surf base depth) is constant on real profiles.

2-DIMENSIONAL NEARSHORE TOPOGRAPHY

The hypothesis here is that the seabed sediment shorewards of surf base is freely redistributed until it comes to equilibrium with an input wave field. It is assumed that the redistribution process occurs essentially in the directions of the wave rays. The profile along any ray is to be calculated according to the methods of the previous section, using eq.(14), and the resulting contour of the breaker zone (approximating to the shoreline) will be therefore dependant on the shape of the surf base contour and the resulting refraction field. The standard ray equation is used, ie.,

$$\Delta\gamma = \sin^{-1}\{(1 + \frac{\Delta C}{C})\sin\gamma\} - \gamma \qquad \ldots\ldots\ldots \qquad (17)$$

(see figure 3a for definitions), where C, ΔC are calculated for the given contour depth and depth change between contours, as normal.

The problem now is as follows. A profile $z(x)$ for any ray path can be calculated by eq.(14), where the local value of H in this equation is subject to eq.(13). The initial direction of the ray is determined by its angle with the assumed surf base contour, and its locus thereafter is modified as it passes each succeeding contour. Inputting a set of parallel rays across an arbitrary surf base contour $s(x,z_s)$ will yield a set of profiles which also define the field of nearshore contours $s(x,z)$, which must be consistent with the set of ray paths themselves. This is approached by iterative calculation, which can be simplified by knowing that locally the contours fall between two relational conditions - either they can locally be parallel in which case the crossing angle γ is altered only by eq.(17), or they can approach a concentric relationship, in which case the crossing angle is modified by an offset ξ, where this is given as shown in figure 3b. For the concentric case (or any case where contours are not locally parallel) there is a similar modification to the refraction coefficient K_r (eq.13). In general, contour relationships will lie between these extremes, and the approach used, to commence iteration, was to assume that the local relationship is such that an offset angle = 0.5ξ applies.

Figure 4 shows a computed example of nearshore topography, for which each ray satisfies eq.(14) subject to eq.(13), and for which the resulting contour positions, on each ray, are consistent between rays and with eq.(17), within the calculation limits (about 5% of each local value, on average). A check on this result can be made by computing the longshore sediment drift, inshore of the breaker line. If the model is correct, lonshore sediment drift, resulting from longshore variations of wave height and approach angle (γ_b) at the breaker line, should be zero. This equilibrium condition is given by Komar (1975) as

$$\frac{1}{c_f}\frac{\partial H_b}{\partial y} = \frac{0.6\,G^3\sin\gamma_b\cos\gamma_b}{1 + \frac{3G^2}{8} - \frac{G^2}{4}\cos^2\gamma_b} \qquad \ldots\ldots\ldots \qquad (18)$$

where $G = H_b/z_b$. Although as Komar (1975) notes, this is an approxi-

Figure 3: DEFINITIONAL SKETCHES, REFRACTION PROCESS

(a) Refraction (eq.17)

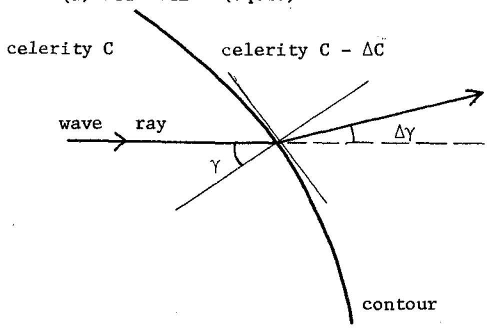

(b) Angular alteration of ray/contour crossing for non-parallel (concentric) contours, used in computing ray paths once a ray passes surf base contour. A bed profile for each ray is computed in similar fashion to figure 2a, and each contour azimuth then is estimated.

$$\xi = \tan^{-1}\left(\frac{\Delta r \tan\gamma}{r + \Delta r}\right)$$

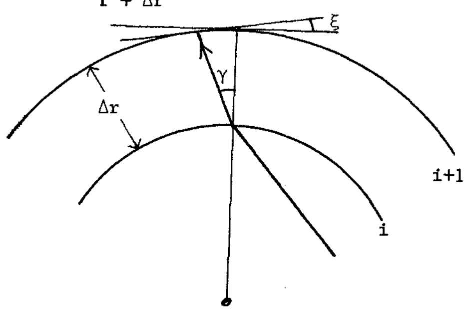

On first iteration it is assumed that crossing angle at contour (i+1) is $\gamma_i - \xi/2$ (see page 7).

FIGURE 4: Self-generated wave-ray and contour field. Input rays (H_{∞} = 2.2m, T = 9sec) incident at input surf-base contour at bottom. On first iteration no correction is made to wave height for refraction coefficient K_r; then K_r

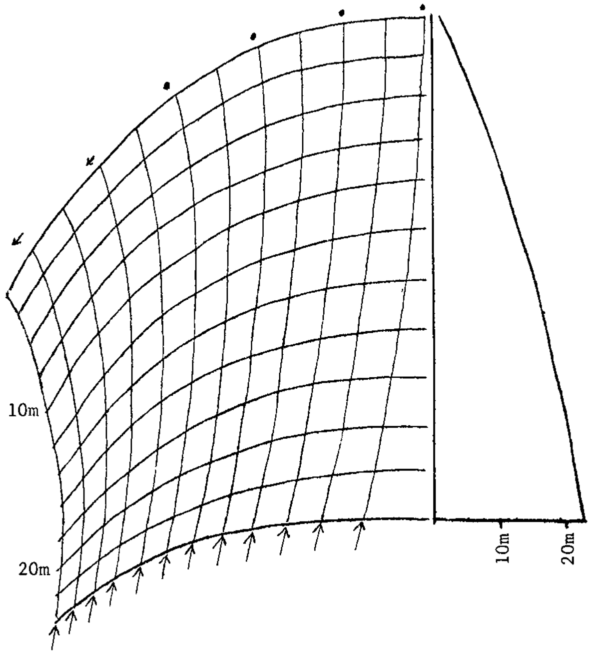

calculated from first iteration is used to correct H at all intersection points, providing basis for second iteration. Figure is plotted from printout of second iteration intersections. Depth profile at right applies to right hand ray. Small arrows at top left show residual longshore current, arising because $\partial H_b/\partial y$ effect exceeds effect of wave obliquity at breaker line (ref. eq.18) (Note that input rays are increasingly closely spaced as surf base contour curvature increases towards left).

mation to the complete solution of the problem,it is well supported by measurements (Komar, op. cit.). When applied to the refraction/topography field in figure 4 this equilibrium condition is approximately met along the model shoreline, although there is a deviation which increases towards the left hand (low energy) end, such that the LHS of eq.(18) exceeds the RHS by about 15%, implying net drift towards the left (shown by small arrows in figure 4). This discrepancy probably reflects the assumption, used in the calculation method, that sediment drift occurs in the direction of a wave ray without a drift component perpendicular to the ray, when its contour-crossing angle is other than 90^{o}. The discrepancy is not large in this simple model calculation, however, and it is concluded that the general approach is sound, although refinements of computational strategy are desirable.

This method, in enabling computation of equilibrium nearshore topography, points the way to predicting the changes which occur when the wave field changes, or when the surf base contour is altered (say by offshore dredging). It is noted that the actual 'equilibrium' topography, developed in any real situation, is the statistical product of a wave climate best expressed in terms of probabilities of wave heights, periods, and directions. An actual topography should be compared with model predictions which embody this consideration. Such a calculation would take into account the variation of surf base contour with wave height and period.

INSHORE EQUILIBRIUM

The sediment drift approach used above for the nearshore region cannot be extended to the inshore area, because in this zone of surf and rip current cells the near bed flow approaches or sometimes even exceeds the critical (Froude number = 1) condition, and sediment moves extensively in suspension. Inshore topography can approximate to a steady state under constant incident waves for more than several days (see Wright, et al., 1979; Chappell and Eliot, 1979, for accounts of inshore states and state changes). The existence of quasi-steady states, with active sediment circulation through longshore and rip current cells, suggests that some parameter in the system is constant, to maintain the condition that grad Q_s = zero (eq.6). Chappell and Eliot (1979)suggested that

$$\text{grad } W = \text{zero} \qquad \ldots\ldots \quad (19)$$

where W is work done on the bed. As noted above (footnote, page 6) this is incorrect in the nearshore, but may approximately be true inshore where depth variation is small, between the primary breaker and the base of the swash. Alternatively, some entropy-like measure may be constant, such as W/h_* (see footnote, page 6), as suggested for fluvial systems by Leopold and Langbein (1962), although it is not clear why this should be so.

There are two approaches to the problem of inshore equilibrium. One is to oppose the gradient effect (eq.9) an estimate of sediment drift in terms of bed friction, as was done for the nearshore. As noted, this is difficult in the absence of a coherent picture of sediment entrainment and drift. The other is to use an assumption such as eq.(19) and then to compute the inshore depth field to satisfy this condition. As it turns out, both approaches yield similar but not identical results. In either case, the local wave height will be subject to

$$H = H_b K_r K_s^* K_f^* \qquad \ldots\ldots\ (20)$$

where K_s^* and K_f^* are shoaling and friction coefficients, respectively, as they apply in the inshore zone (cf. eq.13).Further, as inshore current velocities can be a significant fraction of orbital velocities, work on the bed is

$$W = W_w + W_u \qquad \ldots\ldots\ (21)$$

where the two RHS terms signify wave and current work, respectively.

Inshore waves generally continue to break, to some degree, as they cross the surf zone, although they may locally reform as steep non-breaking waves where they cross the trough. Measurements taken with composite flowmeter and pressure transducer arrays show that inshore waves, between primary break and swash base, show orbital behaviour although not strictly Airy-wave like in form (see data in Wright, et al., 1979; Chappell and Wright, 1978). Hence, a simple paramter θ is introduced to characterise inshore waves, such that

$$H = H_b \int_{x_b}^{x} \theta dx \qquad \ldots\ldots\ (22)$$

where H_b is beaker height an x_b indicates position of the primary breaker line. $\int\theta$ thus is equivalent to K_s^*, and θ itself represents the diminution of effective (orbital) wave motion through the breaking process. In what follows, θ is taken as 0.05/m for spilling waves, 0.1 for plunging waves, and zero for reformed inshore waves. Transition to plunging is taken as G (=wave height/depth) = 1.0, and to spilling when $0.8 < G < 1.0$. These somewhat arbitrary parameters can be better calibrated through field measurements. K_f^* is again given by eq's (7),(8), where $\sinh(kh) \approx kh$.

Total work on the bed, from eq.(21), then becomes

$$W = \delta E + \rho \vec{u}^3 \qquad \ldots\ldots\ (23)$$

where δE is given by eq.(16) and the work by longshore or other current $\vec{u}$ is shown at the second RHS term (cf.eq.1). If eq.(19) applies, then it follows that the local depth must increase in the presence of a current, as δE is depth dependant and total W is constant. This accords qualitatively with the observation that inshore currents are associated with a trough, between primary breaker zone and the shoreline.

Eq's (19) to (23) now are used to compute an inshore topography field, with a shore-parallel train of incident waves. An inshore current is gererated by using the appropriate re-arrangement of eq.(18) (given by Komar, 1975); ie., the current arrises from the inshore radiation stress field generated by longshore

Figure 5: SELF-GENERATED INSHORE MORPHOLOGY AND LONGSHORE CURRENT - RIP CURRENT SYSTEM.

Input H_b = 1.5 m

Surf type: Plunging break or spilling bore + +
Reformed inshore wave - -

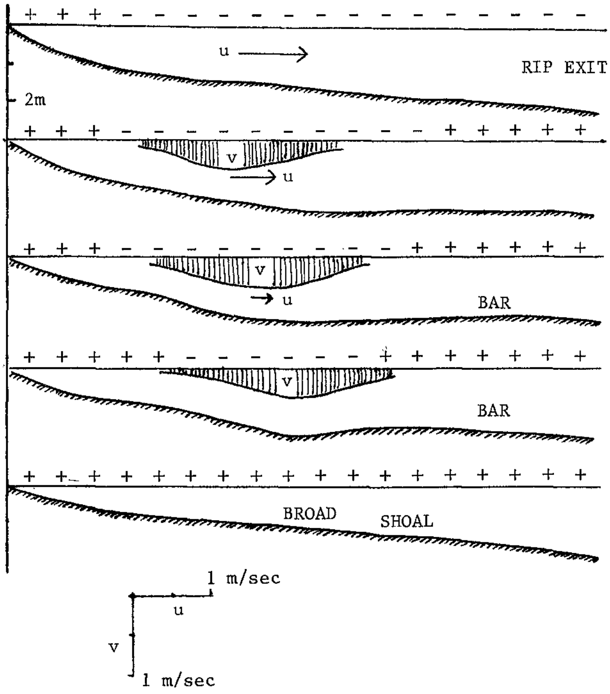

Note: As wave-current interaction is not considered, model does not generate a primary break at rip exit, with parameters used as in text.

variations of wave height. H_b is assumed to vary sinusoidally as a consequence of interaction between incident waves and an inshore stationary edge wave (Bowen, 1969; Chappell and Wright, 1978). A quarter wavelength segment is examined, with a rip located where resultant H_b is a minimum and no longshore current existing at the point where H_b is maximum. No account is taken of inshore refraction arising from wave-current interaction, although this is an important factor (Noda, 1974). The technique used proceeds in two stages. Firstly, the inshore current is calculated from the longshore variation of H_b, and this current is located midway between primary break and shoreline. Profiles across the inshore zone then are computed at 5 positions between the H_b max and $H_b$min positions, using eq's (19) to (23). The resulting radiation stress field then is computed (from the standard equations given by Komar, 1975; 1976), and then, as a second stage, the lonshore current field is recalculated followed by recomputation of the inshore profiles. This iteration reduces divergence between the current field and topography.

Results of the model are shown in figure 5. The 'self-generated' topography emerges as a shallow bar-trough system, which qualitatively agrees well with real inshore circulation-topography systems described as Types 2 and 3 by Wright, et al., (1979).

CONCLUDING DISCUSSION

The models set out in this paper generate nearshore and inshore topography, on mobile sandy beds, with deep water wave H and T as the only input variables, although there are several calibration factors. The models can be criticised as being amalgamations of a number of approximations, some of which are insufficiently tested. Viewed positively, the models produce topographies which appear highly realistic, and offer a method by which changes associated with either variations of wave field, or human alteration of the nearshore-inshore system, can be estimated. The negative side, that undue parameterisation is employed here, can be assessed by reviewing some of these factors.

The main weakness lies with characterisation of sediment drift. To estimate a topographic profile, <u>either</u> explicitly directional wave-induced transport must offset the gradient effect (as in the nearshore case, above), <u>or</u> a non-directional transport function is made everywhere equal, as in the inshore model. The latter suffers from its not being visualisable in terms of fundamental processes; the former, as set out in this paper, suffers in its usage of a naive sediment simplification of sediment drift. This undoubtably can be improved and would affect the result but not the strategy of calculation. A second weakness lies with the approximations used in wave models, particularly in the formulation used for waves in the surf zone. However, assembly of all parameterised factors into a single model focusses attention on areas of weakness. Finally, despite the approximations, the sea bed topography generated by these models appears realistic.

References

Bowen, A.J., 1969. Rip currents. I. Theoretical investigations. Jour. Geophys. Res., 74, 5467-5478.

Bretschneider, C.L., and Reid, R.O., 1954. Modification of wave height due to bottom friction, percolation, and refraction. U.S. Army Corps of Engineers, Beach Erosion Board Tech. Memo., 45.

Brunn, P., 1962. Sea level rise as a cause of shore erosion. A.S.C.E. Waterways and Harbours Divn., 88, 117.

Chappell, J., and Wright, L.D. 1978. Surf zone resonance and coupled morphology. Proc. 16th Coastal Engineering Conf., 1359-1377.

Chappell, J., and Eliot, I.G. 1978. Surf beach dynamics in time and space - an Australian case study, and elements of a predictive model. Marine Geol., 32, 231-250.

Fenton, J.D., and Reinecker, M.M., 1980. Numerical solution of exact equations of water waves. Proc. 17th Coastal Engineering Conf. (this series).

Jonnson, I.G., 1965. Friction Factor Diagrams for Oscillatory Boundary Layers. Basic Res. Rept., 10, Tech. University of Denmark, Copenhagen. 10-21.

Kachel, N.B., and Sternberg, R.W., 1971. Transport of bedload as ripples during an ebb current. Marine Geol., 19, 229-244.

Komar, P.D., 1975. Nearshore currents: generation by obliquely breaking waves and longshore variations in breaker height. In Hails, J., and Carr, A. (eds). Nearshore Sediment Dynamics and Sedimentation (Wiley), 17-46.

Komar, P.D., 1976. Beach Processes and Sedimentation. (Prentice-Hall)., 429pp.

Komar, P.D., and Miller, M.C., 1973. The threshhold of sediment movement under oscillatory water waves. Jour. Sed. Petrol., 43, 1101-1110.

Le Blond, P.H., 1979. An explanation of the logarithmic spiral plan shape of headland-bay beaches. Jour. Sed. Petrol., 49, 1093-1100.

Leopold, L.B., and Langbein, W.B., 1962. The entropy concept in geomorphology. U.S. Geol. Soc. Prof. Paper 500-C.

Longuet-Higgins, M.S., 1953. Mass transport in water waves. Trans. Roy. Soc. London, 245, 525-581.

Neilsen, P., 1979. Some Basic Concepts of Wave Sediment Transport, Inst. Hydrodynamics and Hydraulic Engineering Tech. University of Denmark, Ser.Pap. 20.

Noda, E.K., 1974. Wave-induced nearshore circulation. Jour. Geophys. Res., 79, 4097-4106.

Russell, R.C.H., and Osorio, J.D.C., 1958. An experimental investigation of drift profiles in a closed channel. Proc. 6th Coastal Engineering Conf., 171-183.

Taylor, P.A., and Dyer, K.R., 1977. Theoretical models of flow near the bed and their implications for sediment transport. In Goldberg, E.D., McCave, I.N., O'Brien, J.J., and Steele, J.H. (eds). The Sea: Marine Modelling, v.6.

Wells, D.R., 1967. Beach equilibrium and second-order wave theory. Jour. Geophys. Res., 72, 497-504.

Wright, L.D., Chappell, J., Thom, B.G., Bradshaw, M.P., and Cowell,P.J., 1979. Morphodynamics of reflective and dissipative beach and inshore systems, southeast Australia. Marine Geol., 32, 105-140.

Wright, L.D., Coffey, F.C., and Cowell, P.J., 1980. Nearshore Oceanography and the Morphodynamics of the Broken Bay-Palm Beach Region, N.S.W. Coastal Studies Unit, Dept. Geography, Sydney University, 210pp.